Proceedings of the ASME 2009 Pressure Vessels and Piping Division Conference
PVP2009
July 26-30, 2009, Prague, Czech Republic

PVP2009-77250

EXACT COMPUTATION OF THE AXIAL VIBRATION OF TWO COUPLED LIQUID-FILLED PIPES

Arris S. Tijsseling
Department of Mathematics and Computer Science
Eindhoven University of Technology
P.O. Box 513, 5600 MB Eindhoven
The Netherlands
Phone: +31 40 247 2755
Fax: +31 40 244 2489
E-Mail: a.s.tijsseling@tue.nl

ABSTRACT

A simple recursion is presented that finds exact solutions to the problem of two coupled axially-vibrating liquid-filled pipes. Fluid-structure interaction at pipe ends and junction, and along the pipe because of axial-radial Poisson contraction, is taken into account. The solutions obtained for a waterhammer problem show unprecedented details that resemble noise.

Keywords waterhammer, pipe vibration, fluid-structure interaction, travelling wave, method of characteristics

INTRODUCTION

Strong fluid-structure interaction (FSI) may happen in axially vibrating liquid-filled pipes with closed ends. At the pipe ends, pressure waves in the liquid interact with stress waves in the pipe walls. Such interaction takes also place at unrestrained junctions like pipe diameter changes and elbows (junction coupling). Second and third types of interaction occur along the entire pipe as a result of axial-radial contraction effects (Poisson coupling) and skin friction (friction coupling). The significance of the subject lies in the study of severe waterhammer events and in the altered resonant vibration of liquid-filled pipes [1-3].

A general method is presented that finds exact solutions of the sketched problem if the wave propagations are one-dimensional and non-dispersive. Wave fronts are automatically traced back in time to a given initial situation with the aid of a simple recursion. There are no interpolations, no adjustments of system parameters and no numerical approximations. The strength of the method is the simplicity of the algorithm (recursion) and the accurate (exact) computation of transient events. Its weakness is that the computation time increases exponentially for events of longer duration.

The test problem concerns the axial vibration of two connected, different pipes, where at the junction one incident wave results in two reflected and two transmitted waves. Instantaneous valve closure generates a waterhammer impact load of the pipes. The new exact solution of the transient vibration serves as a benchmark in the verification of numerical results and schemes. Furthermore, the method can be used to perform parameter variation studies without parameter changes generated by the numerical scheme itself (e.g. changed wave speeds or pipe lengths). The present study is a combination and extension of earlier work [4-5]. It gives for the first time exact solutions for FSI in a two-pipe system and as such is a valuable addition to the single-pipe studies [5-6].

MATHEMATICAL MODEL

Skalak [7] presented a four-equation model for the low-frequency acoustic vibration of straight, thin-walled, linearly elastic, prismatic pipes of circular cross-section, filled with inviscid liquid. The four equations, governing fluid velocity, V, fluid pressure, P, axial pipe velocity, $\dot{u}_z$, and axial pipe stress, σ_z, are

$$\frac{\partial V}{\partial t} + \frac{1}{\rho_f}\frac{\partial P}{\partial z} = 0\,, \tag{1}$$

$$\frac{\partial V}{\partial z} + \left(\frac{1}{K} + \frac{2R}{Ee}\right)\frac{\partial P}{\partial t} - \frac{2\nu}{E}\frac{\partial \sigma_z}{\partial t} = 0\,, \tag{2}$$

$$\frac{\partial \dot{u}_z}{\partial t} - \frac{1}{\rho_s}\frac{\partial \sigma_z}{\partial z} = 0\,, \tag{3}$$

$$\frac{\partial \dot{u}_z}{\partial z} - \frac{1}{E}\frac{\partial \sigma_z}{\partial t} + \frac{\nu}{E}\frac{R}{e}\frac{\partial P}{\partial t} = 0\,, \tag{4}$$

where E = Young modulus, e = wall thickness, K = bulk modulus, R = inner pipe radius, t = time, z = distance along pipe, ν = Poisson ratio, ρ = mass density; the subscripts f and s refer to fluid and structure, respectively.

Initial conditions for all four variables, and two boundary conditions at each end of the pipe, complete the mathematical model.

If the Poisson ratio is set equal to zero ($\nu = 0$) the Eqs (1-2) and (3-4) are reduced to classical waterhammer and longitudinal beam equations, respectively. Still, they may be coupled via mutual boundary conditions.

The Eqs (1-4) themselves are energy conserving, but damping can be introduced through the boundary conditions, for example an orifice for the fluid and a dashpot for the structure.

RIEMANN INVARIANTS

Method-of-characteristics (MOC) analysis of the basic Eqs (1-4) reveals the four Riemann invariants

$$\eta_1 = V + \left(\frac{\lambda_1}{\rho_f c_f^2} + \frac{2\nu^2 R}{\rho_s e}\frac{\lambda_1}{c_s^2 - \lambda_1^2}\right)P + \left(2\nu\frac{\lambda_1^2}{c_s^2 - \lambda_1^2}\right)\dot{u}_z - \left(\frac{2\nu}{\rho_s}\frac{\lambda_1}{c_s^2 - \lambda_1^2}\right)\sigma_z\,, \tag{5}$$

$$\eta_2 = V + \left(\frac{\lambda_2}{\rho_f c_f^2} + \frac{2\nu^2 R}{\rho_s e}\frac{\lambda_2}{c_s^2 - \lambda_2^2}\right)P + \left(2\nu\frac{\lambda_2^2}{c_s^2 - \lambda_2^2}\right)\dot{u}_z - \left(\frac{2\nu}{\rho_s}\frac{\lambda_2}{c_s^2 - \lambda_2^2}\right)\sigma_z\,, \tag{6}$$

$$\eta_3 = \left(\rho_f\frac{\nu R}{Ee}\frac{c_f^2\lambda_3^2}{c_f^2 - \lambda_3^2}\right)V + \left(\frac{\nu R}{Ee}\frac{c_f^2\lambda_3}{c_f^2 - \lambda_3^2}\right)P + \left(\frac{\lambda_3^2}{c_s^2}\right)\dot{u}_z - \left(\frac{\lambda_3}{\rho_s c_s^2}\right)\sigma_z\,, \tag{7}$$

$$\eta_4 = \left(\rho_f\frac{\nu R}{Ee}\frac{c_f^2\lambda_4^2}{c_f^2 - \lambda_4^2}\right)V + \left(\frac{\nu R}{Ee}\frac{c_f^2\lambda_4}{c_f^2 - \lambda_4^2}\right)P + \left(\frac{\lambda_4^2}{c_s^2}\right)\dot{u}_z - \left(\frac{\lambda_4}{\rho_s c_s^2}\right)\sigma_z\,, \tag{8}$$

which are constant along the characteristic lines in the distance-time plane with directions $\mathrm{d}z/\mathrm{d}t = \lambda_1$, $\mathrm{d}z/\mathrm{d}t = \lambda_2$, $\mathrm{d}z/\mathrm{d}t = \lambda_3$ and $\mathrm{d}z/\mathrm{d}t = \lambda_4$, respectively. The wave propagation speeds are

$$\lambda_{1,2} = \pm\frac{1}{\sqrt{2}}\left[\gamma^2 - (\gamma^4 - 4c_f^2 c_s^2)^{1/2}\right]^{1/2} \quad \text{and}$$

$$\lambda_{3,4} = \pm\frac{1}{\sqrt{2}}\left[\gamma^2 + (\gamma^4 - 4c_f^2 c_s^2)^{1/2}\right]^{1/2}, \tag{9}$$

where the constants

$$c_f = \left[\frac{\rho_f}{K} + (1 - \nu^2)\frac{2\rho_f R}{Ee}\right]^{-1/2} \quad \text{and} \quad c_s = \left(\frac{E}{\rho_s}\right)^{1/2} \tag{10}$$

are the classical pressure and axial-stress wave speeds, and

$$\gamma^2 = \left(1 + 2\nu^2\frac{\rho_f}{\rho_s}\frac{R}{e}\right)c_f^2 + c_s^2\,. \tag{11}$$

A full derivation of the wave speeds and the Riemann invariants can be found in [5 and 8].

Algebraic inversion of the Eqs (5-8) yields

$$\left(1 - 2\nu^2\frac{\rho_f R}{\rho_s e}\frac{c_f^2}{c_f^2 - \lambda_3^2}\frac{\lambda_1^2}{c_s^2 - \lambda_1^2}\right)V = \left(\frac{\eta_1 + \eta_2}{2}\right) + -2\nu\frac{c_s^2}{c_s^2 - \lambda_1^2}\frac{\lambda_1^2}{\lambda_3^2}\left(\frac{\eta_3 + \eta_4}{2}\right), \tag{12}$$

$$\left(1 - 2\nu^2\frac{\rho_f R}{\rho_s e}\frac{c_f^2}{c_f^2 - \lambda_3^2}\frac{\lambda_3^2}{c_s^2 - \lambda_1^2}\right)P = \frac{\rho_f c_f^2}{\lambda_1}\left(\frac{\eta_1 - \eta_2}{2}\right) + -2\nu\frac{c_s^2}{c_s^2 - \lambda_1^2}\frac{\rho_f c_f^2}{\lambda_3}\left(\frac{\eta_3 - \eta_4}{2}\right), \tag{13}$$

$$\left(1 - 2\nu^2\frac{\rho_f R}{\rho_s e}\frac{c_f^2}{c_f^2 - \lambda_3^2}\frac{\lambda_1^2}{c_s^2 - \lambda_1^2}\right)\dot{u}_z = -\nu\frac{\rho_f R}{\rho_s e}\frac{c_f^2}{c_f^2 - \lambda_3^2}\left(\frac{\eta_1 + \eta_2}{2}\right) + \frac{c_s^2}{\lambda_3^2}\left(\frac{\eta_3 + \eta_4}{2}\right), \tag{14}$$

$$\left(1 - 2\nu^2\frac{\rho_f R}{\rho_s e}\frac{c_f^2}{c_f^2 - \lambda_3^2}\frac{\lambda_3^2}{c_s^2 - \lambda_1^2}\right)\sigma_z = \nu\frac{R}{e}\frac{c_f^2}{c_f^2 - \lambda_3^2}\frac{\rho_f c_f^2}{\lambda_1}\left(\frac{\eta_1 - \eta_2}{2}\right) + -\left(1 + 2\nu^2\frac{\rho_f R}{\rho_s e}\frac{c_f^2}{c_s^2 - \lambda_1^2}\right)\frac{\rho_s c_s^2}{\lambda_3}\left(\frac{\eta_3 - \eta_4}{2}\right). \tag{15}$$

The Eqs (5-9) and (12-15) are summarised in matrix-vector notation by

$$\boldsymbol{\eta}(z,t) = \mathbf{S}^{-1}\boldsymbol{\phi}(z,t) \quad \text{and} \quad \boldsymbol{\phi}(z,t) = \mathbf{S}\,\boldsymbol{\eta}(z,t)\,, \tag{16}$$

where $\boldsymbol{\eta} = (\eta_1, \eta_2, \eta_3, \eta_4)^{\mathrm{T}}$ and $\boldsymbol{\phi} = (V, P, \dot{u}_z, \sigma_z)^{\mathrm{T}}$.

SOLUTION ALGORITHM FOR A SINGLE PIPE

The analysis is in terms of the Riemann invariants η_1, η_2, η_3 and η_4. Therefore, the initial and boundary conditions for V, P, $\dot{u}_z$ and σ_z are translated into Riemann invariants by means of the Eqs (5-8). The solution $\boldsymbol{\eta} = (\eta_1, \eta_2, \eta_3, \eta_4)^{\mathrm{T}}$ in interior point P = (z, t), $0 < z < L$, $0 < t$, in the distance-time plane, is determined by the values of η_1, η_2, η_3 and η_4 generated at the boundary points A_1, A_2, A_3 and A_4, respectively, as displayed in Fig. 1. The value of $\boldsymbol{\eta}$ in the boundary points, at $z = 0$ or $z = L$, is calculated from two compatibility equations, (5, 7) or (6, 8), and two given linear boundary conditions. Because each boundary calculation is mathematically the same, the entire solution can be condensed into a simple recursion. See the Annex. Tracing characteristic lines backwards in time, the recursion stops at time level $t = 0$, where $\boldsymbol{\eta}$ is assigned a known initial value. The general method is fully described and verified in Ref. [5]. At last, solution $\boldsymbol{\eta}(z,t)$ is decomposed into the original variables through the Eqs (12-15).

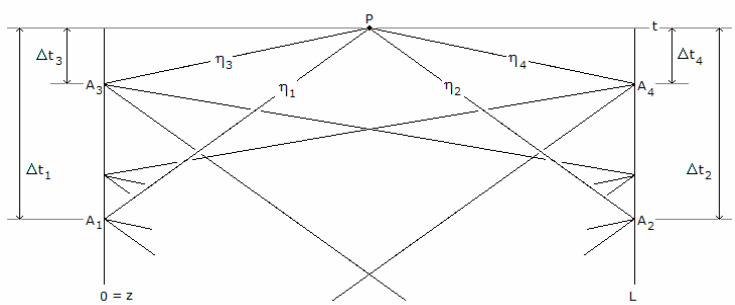

Figure 1. Distance-time plane for single pipe.

SOLUTION ALGORITHM FOR A DOUBLE PIPE

If two different pipes (1 and 2) are connected at $z = z_j$, the local solution vector $\boldsymbol{\eta}$(P) is discontinuous and split into $\boldsymbol{\eta}\mathbf{1}(\mathrm{P}^+)$ and $\boldsymbol{\eta}\mathbf{2}(\mathrm{P}^-)$. The compatibility relations (5-8) provide four equations for the eight unknowns in $\boldsymbol{\eta}(\mathrm{P}^{\pm})$, as seen from Fig. 2, and four additional equations are given by the linear junction condition

$$\mathbf{J1}(t)\ \boldsymbol{\phi}(z_j^-, t) = \mathbf{J2}(t)\ \boldsymbol{\phi}(z_j^+, t) + \mathbf{r}(t) \quad \text{or}$$

$$\mathbf{J1}(t)\ \mathbf{S1}\ \boldsymbol{\eta}\mathbf{1}(z_j, t) = \mathbf{J2}(t)\ \mathbf{S2}\ \boldsymbol{\eta}\mathbf{2}(z_j, t) + \mathbf{r}(t)\ , \qquad (17)$$

where **J1** and **J2** are 4 by 4 coefficient matrices and the vector **r** represents for instance excitation or leakage. The pipe junction is without wave reflection only if $\mathbf{J1}(t)\ \mathbf{S1} = \mathbf{J2}(t)\ \mathbf{S2}$ and $\mathbf{r}(t) = \mathbf{0}$.

Conservation of volume and equilibrium of forces at an axial junction of two pipes, with cross-sectional areas $A1$ and $A2$ of fluid (f) and solid (s), is described herein by the two matrices:

$$\mathbf{J1} = \begin{pmatrix} A1_f & 0 & -A1_f & 0 \\ 0 & 1 & 0 & 0 \\ 0 & 0 & 1 & 0 \\ 0 & A1_f & 0 & -A1_s \end{pmatrix},$$

$$\mathbf{J2} = \begin{pmatrix} A2_f & 0 & -A2_f & 0 \\ 0 & 1 & 0 & 0 \\ 0 & 0 & 1 & 0 \\ 0 & A2_f & 0 & -A2_s \end{pmatrix} \quad \text{and} \quad \mathbf{r}(t) = \mathbf{0}\,. \qquad (18)$$

Separating the unknown values $\boldsymbol{\eta}\mathbf{u} = (\eta 2_1, \eta 1_2, \eta 2_3, \eta 1_4)^{\mathrm{T}}$ from the known values $\boldsymbol{\eta}\mathbf{k} = (\eta 1_1, \eta 2_2, \eta 1_3, \eta 2_4)^{\mathrm{T}}$ at the junction, see Fig. 2, gives the following relation:

$$\boldsymbol{\eta}\mathbf{u} = \mathbf{JSU}^{-1}\ \mathbf{JSK}\ \boldsymbol{\eta}\mathbf{k} \qquad (19)$$

with

$$\mathbf{JSK} = \begin{pmatrix} -(\mathbf{J1\ S1})_{11} & (\mathbf{J2\ S2})_{12} & -(\mathbf{J1\ S1})_{13} & (\mathbf{J2\ S2})_{14} \\ -(\mathbf{J1\ S1})_{21} & (\mathbf{J2\ S2})_{22} & -(\mathbf{J1\ S1})_{23} & (\mathbf{J2\ S2})_{24} \\ -(\mathbf{J1\ S1})_{31} & (\mathbf{J2\ S2})_{32} & -(\mathbf{J1\ S1})_{33} & (\mathbf{J2\ S2})_{34} \\ -(\mathbf{J1\ S1})_{41} & (\mathbf{J2\ S2})_{42} & -(\mathbf{J1\ S1})_{43} & (\mathbf{J2\ S2})_{44} \end{pmatrix} \quad \text{and}$$

$$\mathbf{JSU} = \begin{pmatrix} -(\mathbf{J2\ S2})_{11} & (\mathbf{J1\ S1})_{12} & -(\mathbf{J2\ S2})_{13} & (\mathbf{J1\ S1})_{14} \\ -(\mathbf{J2\ S2})_{21} & (\mathbf{J1\ S1})_{22} & -(\mathbf{J2\ S2})_{23} & (\mathbf{J1\ S1})_{24} \\ -(\mathbf{J2\ S2})_{31} & (\mathbf{J1\ S1})_{32} & -(\mathbf{J2\ S2})_{33} & (\mathbf{J1\ S1})_{34} \\ -(\mathbf{J2\ S2})_{41} & (\mathbf{J1\ S1})_{42} & -(\mathbf{J2\ S2})_{43} & (\mathbf{J1\ S1})_{44} \end{pmatrix}. \qquad (20)$$

Symbolic matrix inversion of the 4 by 4 matrix **JSU** is possible, but not carried out herein because there is no clear advantage over a numerical inversion. Because **J1** and **J2** in Eq. (18) are constant matrices, **JSU** has to be inverted numerically only once.

The solution procedure is tracking wave paths back in time and solving the boundary and junction equations in a recursive way as described for the single pipe. The junction coupling equation (19) is now included in the recursion. The algorithm is given in the Annex.

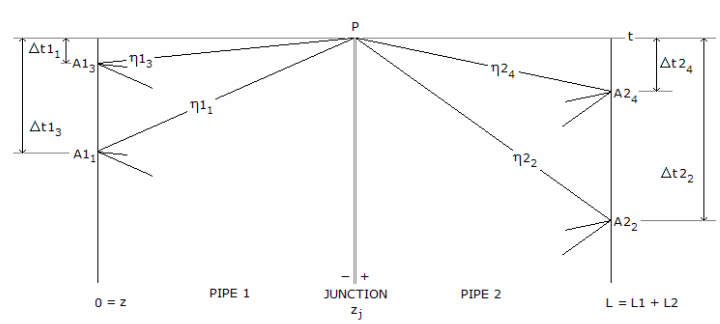

Figure 2. Distance-time plane for double pipe.

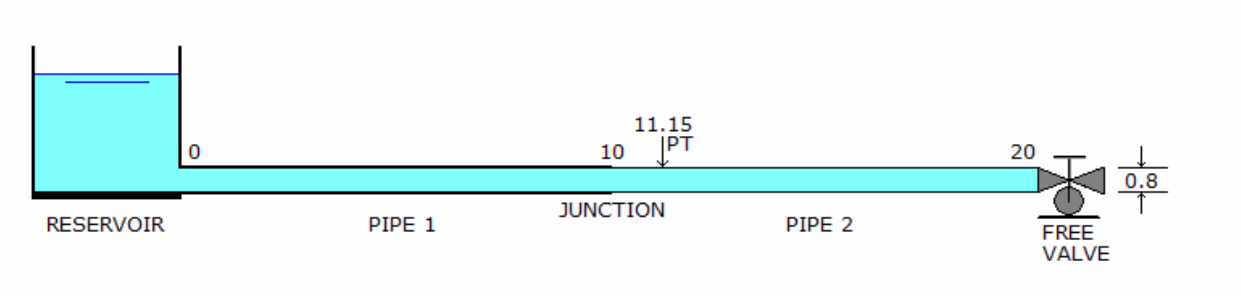

Figure 3. Sketch of test problem; PT = pressure transducer; distances in metres.

Table 1. Input data for the calculation: material and geometrical properties of liquid and pipes.

Liquid	Pipe 1		Pipe 2	
$K = 2.1$ MPa	$L1 = 10$ m	$E1 = 2.1$ GPa	$L2 = 10$ m	$E2 = 2.1$ GPa
$\rho_f = 1000$ kg/m^3	$R1 = 398.5$ mm	$\rho 1_s = 7900$ kg/m^3	$R2 = 398.5$ mm	$\rho 2_s = 7900$ kg/m^3
$Q_0 = 0.499$ m^3/s	$e1 = 16$ mm	$\nu 1 = 0.30$	$e2 = 8$ mm	$\nu 2 = 0.30$

Table 2. Initial liquid velocities (V_0), classical wave speeds (c), coupled wave speeds (λ), and wave travel times (Δt).

Pipe 1	Pipe 2	Relations		Wave travel times
$V1_0 = 1$ m/s	$V2_0 = 1$ m/s	$A1_f V1_0 = A2_f V2_0 = Q_0$		$L1/V1_0 = L2/V2_0 = 10$ s
$c1_f = 1202.1$ m/s	$c2_f = 1049.5$ m/s	$c1_f > c2_f$	$c1_f > \lambda 1_1$	$\Delta t1_1 = L1/\lambda 1_1 = 8.453$ ms
$c1_s = 5155.8$ m/s	$c2_s = 5155.8$ m/s	$c1_s = c2_s$	$c1_s < \lambda 1_3$	$\Delta t2_1 = L2/\lambda 2_1 = 9.759$ ms
$\lambda 1_1 = 1183.0$ m/s	$\lambda 2_1 = 1024.7$ m/s	$\lambda 1_1 > \lambda 2_1$	$c2_f > \lambda 2_1$	$\Delta t1_3 = L1/\lambda 1_3 = 1.909$ ms
$\lambda 1_3 = 5239.1$ m/s	$\lambda 2_3 = 5280.5$ m/s	$\lambda 1_3 < \lambda 2_3$	$c2_s < \lambda 2_3$	$\Delta t2_3 = L2/\lambda 2_3 = 1.894$ ms

CALCULATED RESULTS

The test problem is instantaneous valve closure in the reservoir-pipe-valve system shown in Figure 3. The pipe is 20 m long and divided into two 10 m sections (1 and 2) with different wall thicknesses as specified in Table 1. The wave speeds in each section are different as listed in Table 2 and the used boundary conditions are given in Table 3. Wave reflection will occur at the junction of the two sections. Liquid waves will reflect because of the different wave speeds in the sections and solid waves will primarily reflect because of the difference in cross-sectional wall area. As a result of FSI (junction coupling), one incident wave produces two reflected and two transmitted waves. At the pipe ends, one incident wave generates two reflected waves: at $z = 0$ (fixed reservoir) because of Poisson coupling and at $z = L$ (moving valve) because of junction coupling. The continuous double reflection brings about an exponentially growing number of wave fronts travelling in the system.

The double-pipe algorithm has been tested and successfully verified against two-pipe waterhammer (no junction and Poisson coupling [4]), one-pipe FSI (no junction [5]), and Fortran MOC results obtained with slightly modified wave speeds [9].

Table 3. Boundary conditions.

boundary	$z = 0$	$z = L$ no coupling	$z = L$ FSI coupling
fluid	$P1 = 0$	$V2 = 0$	$V2 = \dot{u}2_z$
pipe	$\dot{u}1_z = 0$	$\dot{u}2_z = 0$	$A2_f P2 = A2_s \sigma 2_z$

Time histories for pressure (P), fluid velocity (V), axial stress (σ_z) and pipe velocity ($\dot{u}_z$) calculated at $z = 11.15$ m are shown in the Figs 4-7. Each graph consists of 1000 points, and results without FSI coupling (frictionless classical waterhammer) are given as a reference.

Figure 4 shows that the maximum pressure predicted by classical waterhammer theory (dashed line) is exceeded considerably because of FSI (continuous line). Furthermore, a precursor travelling roughly at speed c_s is running ahead of the main waterhammer wave which travels roughly at speed c_f. The variations in fluid velocity in Fig. 5, in particular the times of the jumps, are consistent with the variations in pressure in Fig. 4.

The axial pipe stress in Fig. 6 has a large positive value as long as the pressure acting on the free closed end at $z = L$ is large and positive. In principle, the entire solution can be calculated and explained from a detailed wave paths diagram and corresponding jump conditions [10-12]. This tremendous task is carried out automatically by the simple recursion given in the Annex.

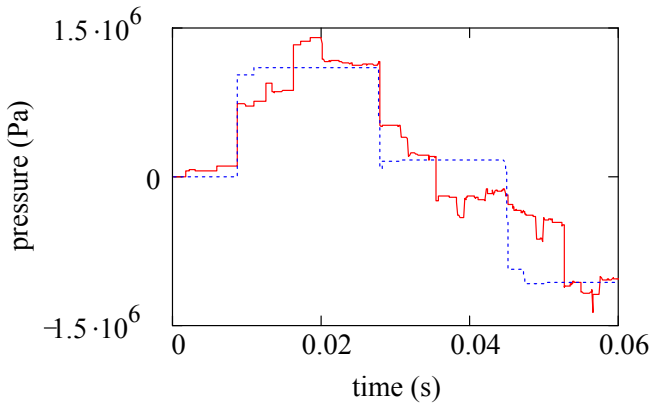

Fig. 4. Pressure history at $z = 11.15$ m. Continuous line: with FSI. Dashed line: classical waterhammer.

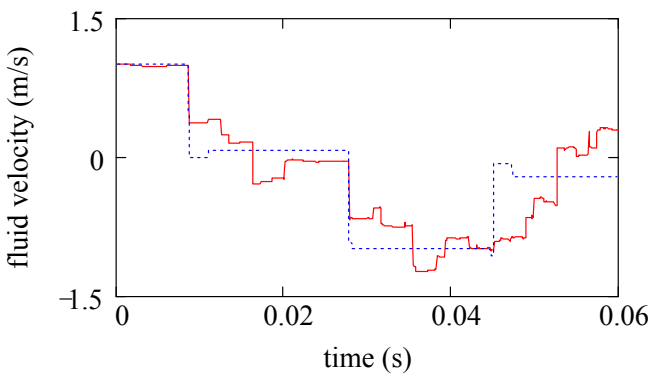

Fig. 5. Fluid velocity history at $z = 11.15$ m. Continuous line: with FSI. Dashed line: classical waterhammer.

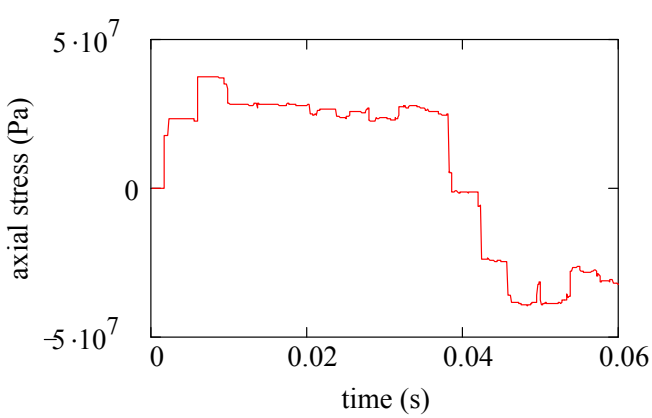

Fig. 6. Stress history at $z = 11.15$ m. Calculation with FSI.

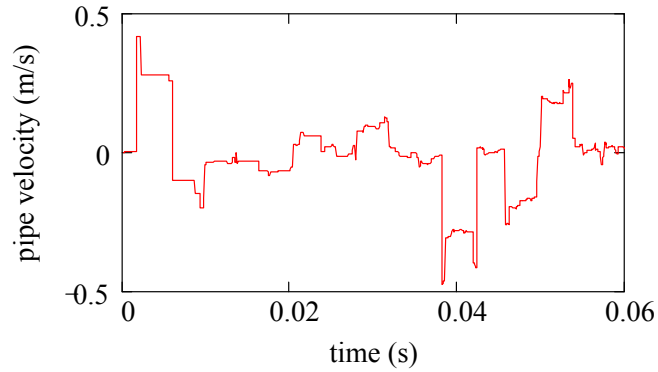

Fig. 7. Pipe velocity history at $z = 11.15$ m. Calculation with FSI.

The Figs 4-7 show an amazing amount of detail. When time increases the calculated traces give the impression to contain noise, but that is not the case: the solutions are exact. In fact, to detect all tiny details, the resolution (the number of points in the graphs) should increase when time advances. This is easy to do, because the method is mesh-free: z and t can be chosen arbitrarily.

The Figs 8-11 show spatial distributions at time $t = 0.03$ s. The main pressure wave, generated by the valve closure at $t = 0$, has reflected from the reservoir and is moving back to the valve (to the right in Figs 8-9). The axial stress in Fig. 10 jumps by a factor two at the junction at $z = L/2$, because the wall areas in pipes 1 and 2 differ by a factor two. The pipe velocity in Fig. 11 is continuous at $z = L/2$.

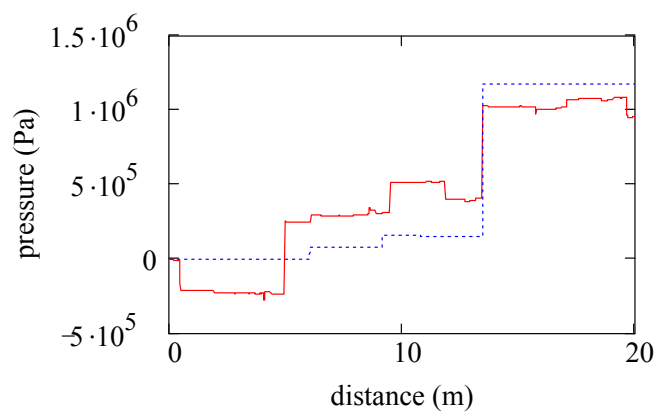

Fig. 8. Pressure distribution at $t = 0.03$ s. Continuous line: with FSI. Dashed line: classical waterhammer.

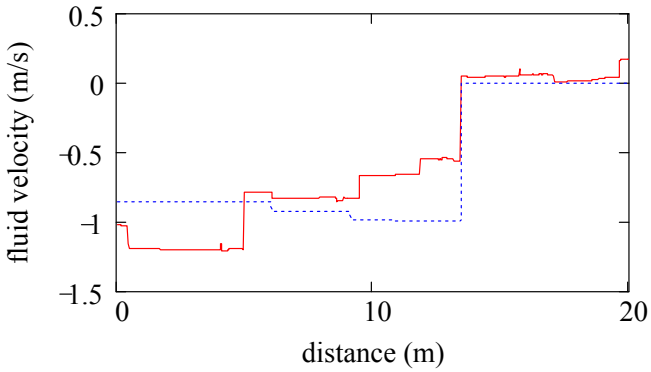

Fig. 9. Fluid velocity distribution at $t = 0.03$ s. Continuous line: with FSI. Dashed line: classical waterhammer.

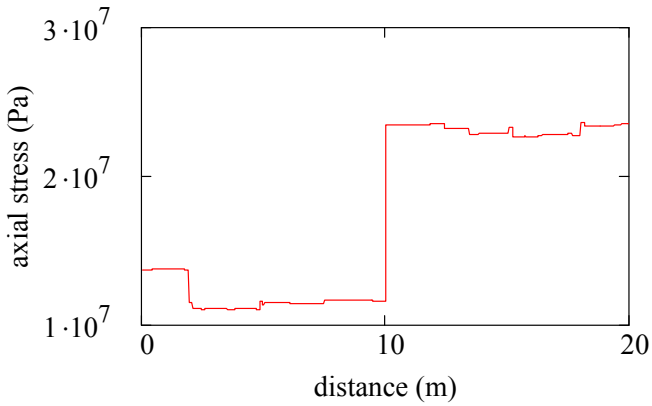

Fig. 10. Stress distribution at $t = 0.03$ s. Calculation with FSI.

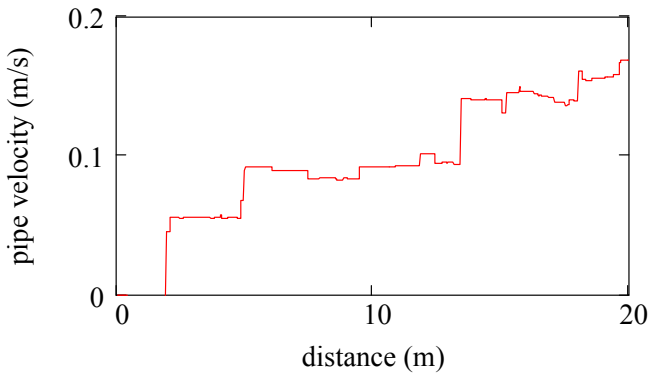

Fig. 11. Pipe velocity distribution at $t = 0.03$ s. Calculation with FSI.

DISCUSSION

The mathematical challenge was to obtain exact solutions in a system with an exponentially growing number of travelling discontinuities. This has been achieved by means of a simple recursion. The solutions presented for waterhammer with FSI in a two-pipe system show an amazing amount of detail, which looks like noise, but is not. In fact, the solutions mimic reality, where small imperfections in otherwise clean laboratory experiments can cause noise-like signals.

The amount of detail in the solutions increases with time, and this calls for non-uniform resolution in the graphs. This can easily be accomplished, even during the calculation, because the method is mesh-free and ideal for adaptivity.

The method is not suitable to simulate events of longer duration; the calculation time is prohibitive. A restart from a highly accurate solution obtained at time $t = T$ may then be an option, that is, restart with initial value $\boldsymbol{\eta}_0 = \boldsymbol{\eta}(z, T)$, where $\boldsymbol{\eta}(z, T)$ has high spatial resolution. This procedure is to the detriment of some smearing, because interpolations are needed to find the restart's initial value for arbitrary z. The restart procedure is expected to work well for gradual valve closure, but for instantaneous valve closure (travelling contact discontinuities) the interpolation error might become unacceptable.

CONCLUSION

The presented method for simulating waterhammer with FSI is able to reveal subtle differences otherwise lost in numerical error, for example deviations due to marginally thicker sections, pipe clamps, small leaks, trapped air pockets, etc. These are minor effects that may accumulate in systems with low damping rates.

The exact solutions are to be used in the verification of numerical schemes.

REFERENCES

[1] Wiggert, D.C., 1996, "Fluid transients in flexible piping systems (a perspective on recent developments)", Proceedings of the 18th IAHR Symposium on Hydraulic Machinery and Cavitation, E. Cabrera, V. Espert, and F. Martínez, eds., Valencia, Spain; Kluwer Academic Publishers, Dordrecht, The Netherlands, ISBN 0-7923-4210-0, pp. 58-67.

[2] Tijsseling, A.S., 1996, "Fluid-structure interaction in liquid-filled pipe systems: a review", Journal of Fluids and Structures **10** (2) 109-146.

[3] Wiggert, D.C., and Tijsseling, A.S., 2001, "Fluid transients and fluid-structure interaction in flexible liquid-filled piping", ASME Applied Mechanics Reviews **54** (5) 455-481.

[4] Tijsseling, A.S., and Bergant, A., 2007, "Meshless computation of water hammer", Scientific Bulletin of the "Politehnica" University of Timişoara, Transactions on Mechanics **52(66)** (6) 65-76, ISSN 1224-6077.

[5] Tijsseling, A.S., 2003, "Exact solution of linear hyperbolic four-equation systems in axial liquid-pipe vibration", Journal of Fluids and Structures **18** (2) 179-196.

[6] Li, Q.S., Yang, K., and Zhang, L., 2003, "Analytical solution for fluid-structure interaction in liquid-filled pipes subjected to impact-induced water hammer", ASCE Journal of Engineering Mechanics **129** (12) 1408-1417.

[7] Skalak, R., 1956, "An extension of the theory of waterhammer", Transactions of the ASME **78** 105-116.

[8] Tijsseling, A.S., 1993, "Fluid-structure interaction in case of waterhammer with cavitation", Ph.D. thesis, Delft University of Technology, Faculty of Civil Engineering, Communications on Hydraulic and Geotechnical Engineering, Report No. 93-6, ISSN 0169-6548, Delft, The Netherlands; http://repository.tudelft.nl/file/264337/201268.

[9] Lavooij, C.S.W., and Tijsseling, A.S., 1991, "Fluid-structure interaction in liquid-filled piping systems", Journal of Fluids and Structures **5** (5) 573-595.

[10] Bürmann, W., 1975, "Water hammer in coaxial pipe systems", ASCE Journal of the Hydraulics Division **101** (6) 699-715. (Errata on p. 1554.)

[11] Williams, D.J., 1977, "Waterhammer in non-rigid pipes: precursor waves and mechanical damping", IMechE Journal of Mechanical Engineering Science **19** (6) 237-242.

[12] Wilkinson, D.H., and Curtis, E.M., 1980, "Water hammer in a thin-walled pipe", Proceedings of the BHRA Third International Conference on Pressure Surges, H.S. Stephens, and J.A. Hanson, eds., Canterbury, UK, pp. 221-240.

[13] Tijsseling, A.S., 2009, "Exact computation of the axial vibration of two coupled liquid-filled pipes", CASA Report 09-xy, ISSN 0926-4507, Department of Mathematics and Computer Science, Eindhoven University of Technology, The Netherlands.

ANNEX

ALGORITHMS

Interior point calculation

The subroutine INTERIOR calculates $\boldsymbol{\eta 1}$ and $\boldsymbol{\eta 2}$ in the interior points of pipe 1 and 2, respectively, from the boundary and junction values. See Figs 1 and 2. Noting that $\lambda 1_2$, $\lambda 1_4$, $\lambda 2_2$ and $\lambda 2_4$ are negative numbers herein, the pseudo-code reads:

```
INTERIOR (input: z, t ; output: η1, η2)
if (0 < z < z_j) then
    CALL BOUNDARY (0, t − z / λ1_1 ; η1, η2)
    η1 := η1_1
    CALL BOUNDARY (z_j, t − (z − z_j) / λ1_2 ; η1, η2)
    η2 := η1_2
    CALL BOUNDARY (0, t − z / λ1_3 ; η1, η2)
    η3 := η1_3
    CALL BOUNDARY (z_j, t − (z − z_j) / λ1_4 ; η1, η2)
    η4 := η1_4
    η1_1 := η1
    η1_2 := η2
    η1_3 := η3
    η1_4 := η4
if (z_j < z < L) then
    CALL BOUNDARY (z_j, t − (z − z_j) / λ2_1 ; η1, η2)
    η1 := η2_1
    CALL BOUNDARY (L, t − (z − L) / λ2_2 ; η1, η2)
    η2 := η2_2
    CALL BOUNDARY (z_j, t − (z − z_j) / λ2_3 ; η1, η2)
    η3 := η2_3
    CALL BOUNDARY (L, t − (z − L) / λ2_4 ; η1, η2)
    η4 := η2_4
    η2_1 := η1
    η2_2 := η2
    η2_3 := η3
    η2_4 := η4
else
    "z is not an interior point"
end
```

Boundary point calculation

The recursive subroutine BOUNDARY calculates $\boldsymbol{\eta 1}$ and $\boldsymbol{\eta 2}$ in the boundary and junction points (finally) from constant initial values $\boldsymbol{\eta 1}_0$ and $\boldsymbol{\eta 2}_0$. See Fig. 2. Noting that $\lambda 1_2$, $\lambda 1_4$, $\lambda 2_2$ and $\lambda 2_4$ are negative numbers herein, the pseudo-code reads:

```
BOUNDARY (input: z, t ; output: η1, η2)
if (t ≤ 0) then
    η1 := η1_0
    η2 := η2_0
else
    if (z = 0) then
        CALL BOUNDARY (z_j, t + z_j / λ1_2 ; η1, η2)
        η2 := η1_2
        CALL BOUNDARY (z_j, t + z_j / λ1_4 ; η1, η2)
        η4 := η1_4
        η1_1 := α12(t) η2 + α14(t) η4 +
              + β11(t) q_1(t) + β13(t) q_3(t)
        η1_2 := η2
        η1_3 := α32(t) η2 + α34(t) η4 +
              + β31(t) q_1(t) + β33(t) q_3(t)
        η1_4 := η4
    if (z = L) then
        CALL BOUNDARY (z_j, t − (L − z_j) / λ2_1 ; η1, η2)
        η1 := η2_1
        CALL BOUNDARY (z_j, t − (L − z_j) / λ2_3 ; η1, η2)
        η3 := η2_3
        η2_1 := η1
        η2_2 := α21(t) η1 + α23(t) η3 +
              + β22(t) q_2(t) + β24(t) q_4(t)
        η2_3 := η3
        η2_4 := α41(t) η1 + α43(t) η3 +
              + β42(t) q_2(t) + β44(t) q_4(t)
    if (z = z_j) then
        CALL BOUNDARY (0, t − z_j / λ1_1 ; η1, η2)
        η1 := η1_1
        CALL BOUNDARY (L, t − (z_j − L) / λ2_2 ; η1, η2)
        η2 := η2_2
```

CALL BOUNDARY $(0,\ t - z_j / \lambda 1_3;\ \boldsymbol{\eta 1}, \boldsymbol{\eta 2})$

$\eta 3 := \eta 1_3$

CALL BOUNDARY $(L,\ t - (z_j - L) / \lambda 2_4;\ \boldsymbol{\eta 1}, \boldsymbol{\eta 2})$

$\eta 4 := \eta 2_4$

$\eta 1_1 := \eta 1$

$\eta 1_2 := \gamma 21(t)\ \eta 1 + \gamma 22(t)\ \eta 2 +$

$+ \gamma 23(t)\ \eta 3 + \gamma 24(t)\ \eta 4 + \delta 2$

$\eta 1_3 := \eta 3$

$\eta 1_4 := \gamma 41(t)\ \eta 1 + \gamma 42(t)\ \eta 2 +$

$+ \gamma 43(t)\ \eta 3 + \gamma 44(t)\ \eta 4 + \delta 4$

$\eta 2_1 := \gamma 11(t)\ \eta 1 + \gamma 12(t)\ \eta 2 +$

$+ \gamma 13(t)\ \eta 3 + \gamma 14(t)\ \eta 4 + \delta 1$

$\eta 2_2 := \eta 2$

$\eta 2_3 := \gamma 31(t)\ \eta 1 + \gamma 32(t)\ \eta 2 +$

$+ \gamma 33(t)\ \eta 3 + \gamma 34(t)\ \eta 4 + \delta 3$

$\eta 2_4 := \eta 4$

if $(z \neq 0 \text{ AND } z \neq L \text{ AND } z \neq z_j)$ then

"z is not at a boundary or junction"

end

Coefficients

The boundary conditions in Table 3 are expressed in terms of general matrix-vector equations in accordance with Ref. [5] by:

$$\mathbf{D} = \begin{pmatrix} 0 & 1 & 0 & 0 \\ 1 & 0 & -1 & 0 \\ 0 & 0 & 1 & 0 \\ 0 & A2_f & 0 & -A2_s \end{pmatrix} \quad \text{and} \quad \mathbf{q} = \mathbf{0}\,.$$

The coefficients α and β determine the unknowns η_1, η_3 and η_2, η_4 at the left and right boundaries, respectively. The coefficients γ and δ determine the unknowns η_2, η_4 and η_1, η_3 at the left and right sides of the junction, respectively. The coefficients α, β, γ and δ are defined in terms of **DS** (**D** multiplied by **S**, see Eq. 16) and $\mathbf{JS} = \mathbf{JSU}^{-1}\,\mathbf{JSK}$ (see Eq. 19) in Table 4.

Implementation

The algorithms have been implemented in Mathcad 11 and 14 and can be found in [13].

Table 4. Coefficients used in the subroutine BOUNDARY.

boundary $z = 0$ in pipe 1	boundary $z = L$ in pipe 2	junction at $z = z_j$
$\det 13 = \mathbf{DS1}_{11}\,\mathbf{DS1}_{33} - \mathbf{DS1}_{31}\,\mathbf{DS1}_{13}$	$\det 24 = \mathbf{DS2}_{22}\,\mathbf{DS2}_{44} - \mathbf{DS2}_{42}\,\mathbf{DS2}_{24}$	$\gamma ij = \mathbf{JS}_{ij}$
$\alpha 12 = \dfrac{-(\mathbf{DS1}_{12}\,\mathbf{DS1}_{33} - \mathbf{DS1}_{13}\,\mathbf{DS1}_{32})}{\det 13}$	$\alpha 21 = \dfrac{-(\mathbf{DS2}_{21}\,\mathbf{DS2}_{44} - \mathbf{DS2}_{24}\,\mathbf{DS2}_{41})}{\det 24}$	$\delta i = (\mathbf{JSU}^{-1}\,\mathbf{r})_i$
$\alpha 14 = \dfrac{-(\mathbf{DS1}_{14}\,\mathbf{DS1}_{33} - \mathbf{DS1}_{13}\,\mathbf{DS1}_{34})}{\det 13}$	$\alpha 23 = \dfrac{-(\mathbf{DS2}_{23}\,\mathbf{DS2}_{44} - \mathbf{DS2}_{24}\,\mathbf{DS2}_{43})}{\det 24}$	
$\alpha 32 = \dfrac{-(\mathbf{DS1}_{32}\,\mathbf{DS1}_{11} - \mathbf{DS1}_{31}\,\mathbf{DS1}_{12})}{\det 13}$	$\alpha 41 = \dfrac{-(\mathbf{DS2}_{41}\,\mathbf{DS2}_{22} - \mathbf{DS2}_{42}\,\mathbf{DS2}_{21})}{\det 24}$	
$\alpha 34 = \dfrac{-(\mathbf{DS1}_{34}\,\mathbf{DS1}_{11} - \mathbf{DS1}_{31}\,\mathbf{DS1}_{14})}{\det 13}$	$\alpha 43 = \dfrac{-(\mathbf{DS2}_{43}\,\mathbf{DS2}_{22} - \mathbf{DS2}_{42}\,\mathbf{DS2}_{23})}{\det 24}$	
$\beta 11 = \dfrac{\mathbf{DS1}_{33}}{\det 13}$	$\beta 22 = \dfrac{\mathbf{DS2}_{44}}{\det 24}$	
$\beta 13 = -\dfrac{\mathbf{DS1}_{13}}{\det 13}$	$\beta 24 = -\dfrac{\mathbf{DS2}_{24}}{\det 24}$ misprint in [5]	
$\beta 31 = -\dfrac{\mathbf{DS1}_{31}}{\det 13}$	$\beta 42 = -\dfrac{\mathbf{DS2}_{42}}{\det 24}$	
$\beta 33 = \dfrac{\mathbf{DS1}_{11}}{\det 13}$	$\beta 44 = \dfrac{\mathbf{DS2}_{22}}{\det 24}$	